2007 IEEE International Conference on
Robotics and Automation
Roma, Italy, 10-14 April 2007

Switched Homography-Based Visual Control of Differential Drive Vehicles with Field-of-View Constraints

G. López-Nicolás[1], S. Bhattacharya[2], J.J. Guerrero[1], C. Sagüés[1] and S. Hutchinson[2]

Abstract— **This paper presents a switched homography-based visual control for differential drive vehicles. The goal is defined by an image taken at the desired position, which is the only previous information needed from the scene. The control takes into account the field-of-view constraints of the vision system through the specific design of the paths with optimality criteria. The optimal paths consist of straight lines and curves that saturate the sensor viewing angle. We present the controls that move the robot along these paths based on the convergence of the elements of the homography matrix. Our contribution is the design of the switched homography-based control, following optimal paths guaranteeing the visibility of the target.**

I. Introduction

Visual control or visual servoing is an extensive field of research, and two interesting surveys on this topic are [14] and [9]. In this paper we consider the problem of visual control of a differential drive vehicle with a monocular vision system on board. The task tackled is the usual approach in which the vehicle is driven from an initial position to the goal. The only information needed by the controller is each current image taken during the navigation and the goal image previously taken at the desired position.

Traditional visual control approaches are based on the epipolar geometry [1], [17], [22], but this model is ill conditioned for planar scenes and is problematic with short baseline. A good alternative is the homography-based approach [2], but existing approaches usually do not take into account the motion constraints of the platform [3], [23] or need the estimation of related-depth parameters [10]. The control scheme proposed here is based on the specific characteristics of the homography matrix elements. Also, this control takes into account the motion constraints of the platform, which is one of our main contributions.

A typical problem in image-based visual servoing is to deal with the field-of-view constraints of the camera [4], [7], [21]. This problem is solved in [8], [19] with hybrid visual servoing approaches. Here we propose to solve it by taking advantage of the research developed in the motion planning field [16], by combining visual control with motion planning [20], [25]. Motion planning approaches usually assume that position information is available, performing the navigation planing task only from pose information, which is not the case of our work.

[1] DIIS-I3A, Universidad de Zaragoza, Spain
{gonlopez, jguerrer, csagues}@unizar.es
[2] Dept. of Electrical and Computer Engineering. Beckman Institute for Advanced Science and Technology. University of Illinois, USA
{sbhattac, seth}@uiuc.edu
This work was supported by projects DPI2006-07928, IST-1-045062-URUS-STP, CCR-0085917 and IIS-0083275.

In our approach, we design a switched controller able to maneuver in order to reach the goal, keeping the target in the camera field of view. For this purpose we benefit from the work presented in [5], where an optimal path scheme is presented. The optimal paths consist of straight lines and curves that saturate the pan angle of the camera. Here, a controller is presented for each type of path. Thus, another contribution is the design of the switched homography-based control following these optimal paths.

The paper is organized as follows. Section II briefly summarizes the work presented in [5] for the design of optimal paths. Section III describes the motion and homography models used in the control. In Sections IV and V, the switched control for straight line and T-curve paths are presented respectively. Conclusions are discussed in Section VI. In Appendix A we present the criterion for the selection of the type of optimal paths required depending on the initial configuration.

II. Optimal Paths

In this section we briefly summarize the work presented by Bhattacharya et al in [5]. They consider the problem of planning shortest paths for differential drive robots whose motion is further constrained by sensing considerations. In particular, they consider the case when the robot must maintain visibility of a fixed landmark using a body-mounted camera with a limited field of view. Kantor and Rizzi [15] have considered a similar problem from a control theoretic perspective. They have proposed a framework for the construction of globally convergent, purely feedback-based controllers for such a system using the idea of variable constraint control [11] [12].

Their primary result is that the shortest paths for this system consist of straight line segments or curves that saturate the sensor viewing angle, which lead to logarithmic spirals. These are called the T-curves. Since the camera is allowed to rotate in a closed interval $[\phi_1, \phi_2]$, two kinds of T-curves can be drawn from each point. The T-curves generated by saturating the camera angle at ϕ_1 are called T1 curves and the T-curves generated by saturating the camera angle at ϕ_2 are called T2 curves. The T1 and T2 curves passing through a point P are denoted by $T1_P$ and $T2_P$ respectively. An example is shown in Fig. 1. In the current work, instead of a camera which can rotate to keep the target in the centre of the image, we use for simplicity a fixed camera where the target is allowed to move from one side of the image to the other, restricted to the field-of-view constraint $[\phi_1, \phi_2]$.

1-4244-0602-1/07/$20.00 ©2007 IEEE.

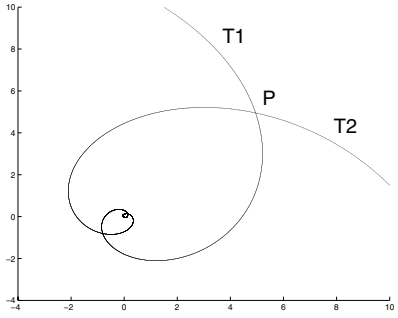

Fig. 1. A T1 and T2 curve generated from a point P.

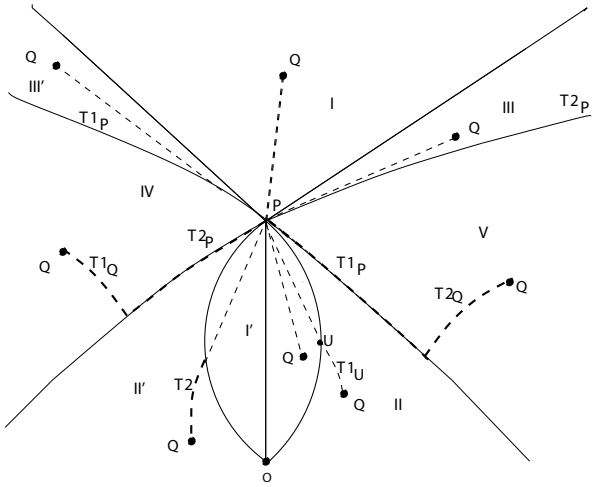

Fig. 2. Regions and shortest paths. The Initial position is P, the different goals are denoted by Q and the observed target is O.

Figure 2 shows the final partition of the workspace into regions according to the nature of optimal paths. The shortest paths from P to any point Q in regions I and I' are straight lines. The shortest paths in region II consist of a straight line followed by T1 curve. The shortest paths in region II' consist of a straight line followed by a T2 curve. The shortest paths from P to any point Q in region III consist of a T2 curve, followed by a straight line. The shortest paths from P to any point in region III' are a straight line followed by T1 curve. The shortest paths from P to any point in region IV consist of a T2 curve and then a T1 curve. The shortest paths from P to any point in region V consist of a T1 curve and then a T2 curve. In the current work we present the criteria for deducing in which region is the robot (Appendix A).

III. Motion and Geometric Model

The kinematics of a differential drive vehicle expressed as a function of the robot velocities (v, ω), with $(x, z, \phi)^T$ the position and orientation of the vehicle, are:

$$\begin{pmatrix} \dot{x} \\ \dot{z} \\ \dot{\phi} \end{pmatrix} = \begin{pmatrix} \sin\phi \\ \cos\phi \\ 0 \end{pmatrix} v + \begin{pmatrix} 0 \\ 0 \\ 1 \end{pmatrix} \omega \ . \qquad (1)$$

Two perspective images can be geometrically linked by a homography. This homography relates corresponding points between the images belonging to a plane. Let us suppose the two images are taken with the same camera, whose projection matrixes are $\mathbf{P}_1 = \mathbf{K}[\mathbf{I}|\mathbf{0}]$ and $\mathbf{P}_2 = \mathbf{K}[\mathbf{R}|-\mathbf{Rc}]$, being $\mathbf{R}$ the camera rotation, $\mathbf{c}$ the translation between the cameras, and $\mathbf{K}$ the camera calibration, determined by the focal length in pixel dimensions (α_x, α_y). In practice, we assume that the principal point is in the centre of the image ($x_0 = 0$, $y_0 = 0$) and that there is no skew ($s = 0$).

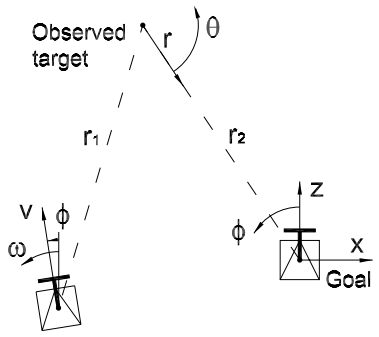

Fig. 3. References in Polar and Cartesian coordinates.

A homography $\mathbf{H}$ can be related to motion:

$$\mathbf{H} = \mathbf{K}\left(\mathbf{R} - \mathbf{t}\frac{\mathbf{n}^T}{d}\right)\mathbf{K}^{-1} = \mathbf{KR}\left(\mathbf{I} + \mathbf{c}\frac{\mathbf{n}^T}{d}\right)\mathbf{K}^{-1} , \qquad (2)$$

where $\mathbf{n} = (n_x, n_y, n_z)^T$ is the normal of the plane and d is the distance between the plane and the reference. We consider a mobile robot moving in a planar surface (Fig. 3),

$$\mathbf{R} = \begin{bmatrix} \cos\phi & 0 & \sin\phi \\ 0 & 1 & 0 \\ -\sin\phi & 0 & \cos\phi \end{bmatrix} \textit{ and } \ \mathbf{c} = (x, 0, z)^T \ .$$

Therefore, the homography of planar motion is $\mathbf{H} = h_{ij}$, $(i, j = 1, 2, 3)$ where $h_{21} = 0$, $h_{22} = 1$ and $h_{23} = 0$. Elements h_{21}, h_{22} and h_{23} do not give information because of the planar motion constraint. Developing expression (2) we obtain the homography elements as a function of the system parameters:

$$\begin{cases} h_{11} = \cos\phi + (x\cos\phi + z\sin\phi)\frac{n_x}{d} \\ h_{12} = \frac{\alpha_x}{\alpha_y}(x\cos\phi + z\sin\phi)\frac{n_y}{d} \\ h_{13} = \alpha_x\left(\sin\phi + (x\cos\phi + z\sin\phi)\frac{n_z}{d}\right) \\ h_{31} = \frac{1}{\alpha_x}\left(-\sin\phi + (-x\sin\phi + z\cos\phi)\frac{n_x}{d}\right) \\ h_{32} = \frac{1}{\alpha_y}(-x\sin\phi + z\cos\phi)\frac{n_y}{d} \\ h_{33} = \cos\phi + (-x\sin\phi + z\cos\phi)\frac{n_z}{d} \end{cases} \qquad (3)$$

The control presented uses the homography elements h_{11}, h_{13} and h_{33}; and the analysis of these homography elements lead to the design of the control law. Elements h_{31} and h_{32} are discarded because of its sensitivity to noise compared with the rest of the elements, given that they are smaller because of the factors $1/\alpha_x$ and $1/\alpha_y$ appearing in h_{31} and h_{32} respectively. Besides, in human environments, vertical planes are common, therefore we avoid using elements depending directly on n_y, like h_{12}. Moreover, planes in front of the camera are more easily detected, so in general, we can consider that the normal of the plane detected has $n_z \neq 0$.

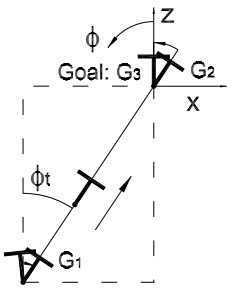

Fig. 4. Diagram of the three steps for the straight line path.

IV. Switched Control for Straight Line Paths

In this section we present the image-based visual control for the straight line motion, taking advantage of this specific trajectory. In this path we propose a control law decoupling rotation and translation. The resulting path of this motion is shown in Fig. 4.

The motion is divided into three sequential steps. In the first step the robot rotates until the camera points to the goal position. In the second step, the robot performs a straight line translation with a constant angle with respect to the global reference ($\phi = \phi_t$) until the goal position. Finally, in the third step, the orientation is corrected by rotating about the robot axis. The key point is to establish the conditions that have to be held during each phase of the navigation. In our reference system we have that $x = -z\tan\phi_t$. Using this expression in (3), the particular form of the homography that is held at the end of first step and during the second step is:

$$\mathbf{H}_{(\phi=\phi_t)} = \begin{bmatrix} \cos\phi_t & 0 & \alpha_x \sin\phi_t \\ 0 & 1 & 0 \\ \frac{-\sin\phi_t}{\alpha_x} + \frac{zn_x/d}{\alpha_x\cos\phi_t} & \frac{zn_y/d}{\alpha_y\cos\phi_t} & \frac{\cos^2\phi_t + zn_z/d}{\cos\phi_t} \end{bmatrix} \quad (4)$$

At the end of the second step the robot has an orientation error and no translation error ($x = 0, z = 0, \phi = \phi_t$). Then, the matrix that results at the end of the second step is given by

$$\mathbf{H}_{(x=0,z=0,\phi=\phi_t)} = \begin{bmatrix} \cos\phi_t & 0 & \alpha_x \sin\phi_t \\ 0 & 1 & 0 \\ \frac{-\sin\phi_t}{\alpha_x} & 0 & \cos\phi_t \end{bmatrix} . \quad (5)$$

Finally, at the end of the navigation, when the robot reaches the goal pose, the homography will be the identity matrix, $\mathbf{H}_{(x=0,z=0,\phi=0)} = \mathbf{I}$.

In this method, we suppose that the intrinsic camera calibration matrix is known and therefore the value of the focal length α_x is given. This control is based on the key value ϕ_t, which is unknown. From (4) we have that $h_{11} = \cos\phi_t$ and $h_{13} = \alpha_x \sin\phi_t$ and then, we can obtain the next equation, which is true when $\phi = \phi_t$,

$$h_{11}^2 + \frac{h_{13}^2}{\alpha_x^2} = 1 . \quad (6)$$

The orientation ϕ_t during the first step is reached with (6) and, supposing there is odometry drift or noise, we use the same expression during the second step to maintain this orientation ϕ_t. At the end of the second step we have $h_{11} = h_{33}$, this is used to set v during this step. When the robot is over the target up to a rotation, h_{13} becomes zero as the desired orientation is reached. Thus, we define the switched control as:

Step 1: $v = 0,\ \omega = -k_\omega(h_{11}^2 + h_{13}^2/\alpha_x^2 - 1)$.
Step 2: $v = -k_v(h_{11} - h_{33}),\ \omega = -k_\omega(h_{11}^2 + h_{13}^2/\alpha_x^2 - 1)$.
Step 3: $v = 0,\ \omega = -k_\omega h_{13}$.

The control gains are k_ω and k_v, with $k_v > 0$. In the third step $k_\omega > 0$, while the sign of k_ω in the first and second step has to be selected at the beginning of the motion. For example, using plane parallax we can easily know the sign of the x-coordinate of the robot position and determine the correct sign of k_ω. The control law proposed does not need to know the value of ϕ_t. Literature on this controller can be found in [18].

A. Stability Analysis

We define the common Lyapunov function expressing the robot position in polar coordinates $(r(t), \theta(t), \phi(t))$, with the reference origin in the observed target and θ positive from z-axis anticlockwise (Fig. 3), as

$$V = V_r + V_\theta + V_\phi = \frac{(r - r^{G_i})^2}{2} + \frac{(\theta - \theta^{G_i})^2}{2} + \frac{(\phi - \phi^{G_i})^2}{2} \quad (7)$$

where r^{G_i}, θ^{G_i} and ϕ^{G_i} denote the desired value of the parameter in the subgoal position of each step (G_1, G_2 and G_3). This candidate function is positive definite. After differentiating we obtain:

$$\dot{V}_r = (r - r^{G_i})\, v \cos(\phi - \theta) . \quad (8)$$

$$\dot{V}_\theta = (\theta - \theta^{G_i})\, \frac{v}{r} \sin(\phi - \theta) . \quad (9)$$

$$\dot{V}_\phi = (\phi - \phi^{G_i})\, \omega . \quad (10)$$

Now we analyze the derivative Lyapunov candidate function of each step to show it is strictly negative. This analysis is valid whether if the goal is behind or in front of the initial position.

1) Step towards G_1: Here the robot performs a rotation with $v = 0$, thus, we only need to consider $\dot{V} = \dot{V}_\phi$. The desired orientation is $\phi^{G_1} = \phi_t$. $\dot{V}_\phi < 0$ is guaranteed if $(\phi - \phi^{G_1}) > 0$ and then $\omega < 0$; or else, if $(\phi - \phi^{G_1}) < 0$ and then $\omega > 0$. In this step, the sign of ω is guaranteed to be correct, given that the sign of k_ω is selected as explained previously.

2) Step towards G_2: In step 2 the robot moves towards the target in a straight line motion with $\theta^{G_2} = \theta$. Thus, we define $\dot{V} = \dot{V}_r + \dot{V}_\phi$. The sign of $(r - r^{G_2})$ is always positive. Then, with $\cos(\phi - \theta) < 0$ we have $v > 0$ and with $\cos(\phi - \theta) > 0$ we have $v < 0$. The velocity given by the control and with (4) is $v = k_v z n_z/(d\cos\phi_t)$, which gives the expected signs. With $\dot{V}_\phi$ we have the same reasoning of step 1.

3) Step towards G_3: Similar than step 1, in this case, the sign of ω can be easily checked taking into account that $\phi^{G_3} = 0$ and $h_{13} = \alpha_x \sin\phi_t$. Therefore $\dot{V} < 0$.

Therefore $\dot{V} < 0$ in all the steps. We have also asymptotic stability given that $\dot{V}$ is negative definite in all the steps.

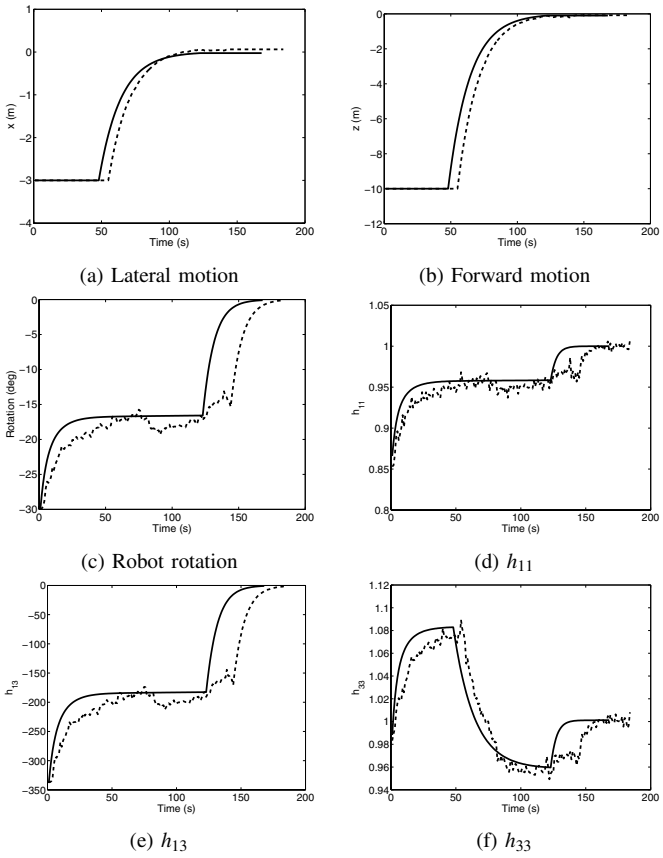

(a) Lateral motion (b) Forward motion

(c) Robot rotation (d) h_{11}

(e) h_{13} (f) h_{33}

Fig. 5. Simulations following a straight line path with and without image noise of $\sigma = 0.3$ pixels (dotted and solid line respectively).

B. Simulation Results: Straight Line Paths

Simulations showing the performance of the switched control law following a straight line path are presented. A virtual framework is used by generating random 3D points in a planar scene. The 3D points of the scene are projected in the image plane through a virtual camera. The size of the images obtained from the virtual camera is 640×480 and $\phi_1 = 26.56^\circ$, $\phi_2 = -26.56^\circ$. The homography between the current and goal image is computed from the image point matches [13].

The initial position of the robot in the simulations of Fig. 5 is (x (m), z (m), θ (deg)) = $(-3, -10, -30^\circ)$ and the target position is $(0, 0, 0^\circ)$. Two simulations are superposed in the graphics, one without noise and the other adding white image noise to points in the image with standard deviation of $\sigma = 0.3$ pixels. For the case of noisy image points, the final position is $(0.062, -0.080, -0.094^\circ)$. The simulations show that the method works properly in spite of image noise.

V. Switched Control following T-curves

In this section we present a switched control law that moves the robot on T-curves, as summarized in Section II. The motion is divided into five sequential steps (Fig. 6), and the target is the plane that generates the homography. For each step we define a subgoal in terms of homography parameters. This is a position based approach, given that we need to get the orientation and the ratio of the robot position from the homography decomposition to define the subgoals.

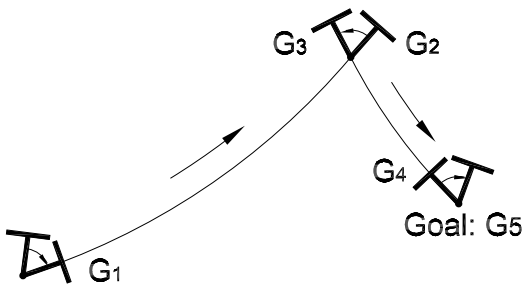

Fig. 6. Diagram of the designed path consisting in five steps.

The control proposed for each step is:

Step 1: $v = 0,\ \omega = -k_\omega (h_{13} - h_{13}^{G_1})$.

Step 2: $v = -k_v (h_{33} - h_{33}^{G_2}),\ \omega = -k_\omega (h_{13} - h_{13}^{G_2})$.

Step 3: $v = 0,\ \omega = -k_\omega (h_{13} - h_{13}^{G_3})$.

Step 4: $v = -k_v (h_{33} - h_{11}),\ \omega = -k_\omega (h_{13} - h_{13}^{G_4})$.

Step 5: $v = 0,\ \omega = -k_\omega (h_{13} - h_{13}^{G_5})$.

The control gains are k_v and $k_\omega > 0$. The sign of k_v depends on the type of optimal path required, if it starts with a T2 curve $k_v > 0$, else $k_v < 0$ (see Appendix A). h_{11}, h_{13} and h_{33} are the corresponding elements of the homography between the current and goal position. $h_{13}^{G_i}$ and $h_{33}^{G_i}$ are defined from the homography between the desired subgoal of the step i and the goal position. From equation (3), the parameters $h_{13}^{G_i}$ and $h_{33}^{G_i}$ can be calculated as

$$h_{13}^{G_i} = \frac{(\frac{h_{13}}{\alpha_x} - \sin\phi)(\rho^{G_i}\cos\phi^{G_i} + \sin\phi^{G_i})}{(\rho\cos\phi + \sin\phi)\rho_z / \alpha_x} + \alpha_x \sin\phi^{G_i}, \quad (11)$$

$$h_{33}^{G_i} = \frac{(h_{33} - \cos\phi)(-\rho^{G_i}\sin\phi^{G_i} + \cos\phi^{G_i})}{(-\rho\sin\phi + \cos\phi)\rho_z} + \cos\phi^{G_i}, \quad (12)$$

where $\rho = x/z$, $\rho^{G_i} = x^{G_i}/z^{G_i}$ and $\rho_z = z/z^{G_i}$. The current robot orientation is ϕ and the desired orientation in each step is ϕ^{G_i}.

Now we define the values of $h_{13}^{G_i}$ and $h_{33}^{G_i}$ for each subgoal:

1) Subgoals G_1, G_3 and G_5: The steps 1 and 3 consist in rotating the robot until it has the orientation of the corresponding T-curve. Since $v = 0$ in these steps, $\rho^{G_1} = \rho$, $\rho^{G_3} = \rho$ and $\rho_z = 1$ in (11) and (12). The desired orientations in these steps are $\phi^{G_1} = \phi + \arctan(\frac{p_x}{\alpha_x} + \phi_2)$ and $\phi^{G_3} = \phi + \arctan(\frac{p_x}{\alpha_x} + \phi_1)$, where p_x is the x-coordinate of a point of the target in the current image and $[\phi_1, \phi_2]$ are the extremities of the camera field of view. In step 5 the robot performs a rotation to converge the homography matrix to identity, therefore $h_{13}^{G_5} = 0$.

2) Subgoal G_4: In step 4 the robot moves backwards until it reaches the goal position (with the T-curve orientation). In this step, we require h_{33} to converge to h_{11}, see (5). Up to odometry drift we suppose that the robot follows the desired path, so $\rho^{G_4} = \rho$ and $\rho_z = 1$ and the desired orientation is $\phi^{G_4} = \phi + \arctan(\frac{p_x}{\alpha_x} + \phi_1)$.

3) Subgoal G_2: After step 1 the robot is on a T-curve and the new subgoal is the intersection point between the two T-curves. In step 2 we have the same reasoning as step 4 for $h_{13}^{G_2}$ having $\rho^{G_2}=\rho$, $\rho_z=1$ and $\phi^{G_2}=\phi+\arctan(\frac{p_x}{\alpha_x}+\phi_2)$. For $h_{33}^{G_2}$, we have $\phi^{G_2}=\theta^{G_2}+\phi_2$, where ϕ^{G_2} is computed in the following way: From the equations of the T-curves (see (14) in Appendix A) we can deduce that at the end of the second step

$$\theta^{G_2}=\frac{\ln(r_1/r_2)+(\theta_1/\tan\phi_1-\theta_2/\tan\phi_2)}{1/\tan\phi_1-1/\tan\phi_2}\,, \qquad (13)$$

where the ratio r_1/r_2 (see Fig. 3) can be computed as

$$\frac{r_1}{r_2}=\frac{\rho_{12}\cos(\gamma_2)+\sin(\gamma_2)}{\rho_{12}\sin(\beta)-\cos(\beta)}\,,$$

with $\gamma_2=\arctan(\frac{p_{x2}}{\alpha_x})$ and $\beta=\pi/2+\phi_2-\theta_{12}$, with $\rho_{12}=\rho^{G_1}$ the ratio between initial and goal position and θ_{12}:

$$\theta_{12}=\theta_2-\theta_1=\gamma_1-\gamma_2-\phi_{12}\,,$$

where $\gamma_1=\arctan(\frac{p_{x1}}{\alpha_x})$, and ϕ_{12} is the relative orientation between initial and goal position obtained from the homography decomposition [24]. p_{x1} and p_{x2} are the x-coordinate of a point on the target in the initial and goal images respectively. We have fixed our reference at $\theta_2=0$.

For $h_{33}^{G_2}$ we can compute neither ρ^{G_2} nor ρ_z because we need the value of ρ in the subgoal position of step 2 which can only be known when this position is reached. We use the following approximation instead: $\rho^{G_2}=\rho$ and $\rho_z=1$, with ρ defined in the current position. The previous simplification only becomes true as the robot approaches the second subgoal. Simulations show that the approximation for $h_{33}^{G_2}$ does not affect the convergence or accuracy of the method. This is because this parameter is responsible for stopping the robot in the subgoal. As the robot approaches the subgoal, given that the orientation is properly corrected, this parameter is more exact. In fact, we present a successful implementation of the extreme case in which range constraints are considered (Section V-B) and then, the system needs to switch to next step before reaching the subgoal. Angles ϕ_1 and ϕ_2 can be exchanged in the previous equations depending on the type of optimal path selected (Appendix A).

A. Stability Analysis

The stability of each step is analyzed defining the corresponding Lyapunov candidate functions:

1) Steps towards G_1, G_3 and G_5: These steps consist in pure rotations and the Lyapunov candidate function is defined as $\dot{V}=\dot{V}_\phi$, see (10). If $(\phi-\phi^{G_i})>0$, $\omega<0$. Else, if $(\phi-\phi^{G_i})<0$, $\omega>0$. Therefore $\dot{V}<0$.

2) Steps towards G_2 and G_4: We define the Lyapunov candidate function $V=V_r+V_\phi$, see (8) and (10). The analysis of V_ϕ in steps 2 and 4 is the same as steps 1, 3 and 5. With respect to V_r: $V_r<0$ is guaranteed if the robot moves in step 2 in a T1 curve ($v>0$), given that $(r-r^{G_2})>0$ and $\cos(\phi-\theta)<0$. If the robot moves backwards ($v<0$) in step 4 in a T2 curve, we have $(r-r^{G_4})<0$ and $\cos(\phi-\theta)<0$, and again $V_r<0$. Therefore, $\dot{V}<0$ in steps 2 and 4.

We have also that the stability is asymptotic given that $\dot{V}$ is negative definite in all the steps. The previous development needs the analysis of the signs of the velocities given by the control law for each step. Given that this is not a trivial check, we use an approximation for the verification. In (11) we suppose that $(\rho^{G_i}\cos\phi^{G_i}+\sin\phi^{G_i})\simeq(\rho\cos\phi+\sin\phi)$ and in (12) that $(-\rho^{G_i}\sin\phi^{G_i}+\cos\phi^{G_i})\simeq(-\rho\sin\phi+\cos\phi)$ and that $\rho_z\simeq 1$. Actually, this approximation only becomes true as the robot approaches to each subgoal. With this simplification we have that $v\simeq -k_v(\cos\phi-\cos\phi^{G_i})$ and $\omega\simeq -k_\omega\alpha_x(\sin\phi-\sin\phi^{G_i})$.

Before starting the navigation, we need to select what method is needed (Section IV or V). The selection procedure is presented in Appendix A, and then, the selected control is carried out to reach the goal. But if there is noise or drift a final error can be obtained due to the motion constraint in such a way that $\mathbf{H}\neq\mathbf{I}$ at the end of the motion. In this case, the procedure can be repeated until $\mathbf{H}=\mathbf{I}$. In order to ensure the stability of the global control we use the notion of stability of switched systems presented in [6]. This means that we need the global switching system to fulfil the *sequence nonincreasing condition* to ensure stability. We define the Lyapunov function: $V=V_r$. It has been shown that $\dot{V}_r<0$ for both methods presented here. Therefore, for the global switched control we have $\dot{V}<0$, and then the system is stable in the Lyapunov sense.

B. Simulation Results: T-curve Paths

In this section we present several simulations showing the performance of the switched control following T-curves. The robustness of the approach is tested considering image noise and odometry drift. In all the simulations the initial position is (x, z, θ) = $(-9,-2,-20^\circ)$ and the goal position is $(0,0,0^\circ)$. The target, that must be kept in the camera field of view is located in (x, z) = $(-3,8)$. In our homography-based approach the target is the plane that generates the homography. Figure 7 shows the results using our approach without noise and Fig. 8 shows the results when adding white noise to the image points with standard deviation of $\sigma=1$ pixel. Different graphics are shown, like the path followed by the robot and its coordinates along the time, the velocities (v,ω), or the evolution of the homography elements used in the control. In Fig. 8(c), we show the x-coordinate in the image of a point of the target. The field-of-view limit is 320 pixels. It can be seen in the figure that the point does not leave the field of view (in practise a threshold should be used). In simulation of Fig. 9(a) we have added odometry drift of 0.8 deg/m to the robot motion. It can be seen that, after two iterations, the system converges to the goal with good accuracy.

The previous method can be easily extended to the case when camera range constrains exist. For example, when there is a minimum distance (r_{min}), below which the target can not be seen in the image (for example because of its size) or there is a maximum distance (r_{max}) above which the target cannot be seen properly (for example because of camera resolution). If one of these limits is reached, the system switches to the

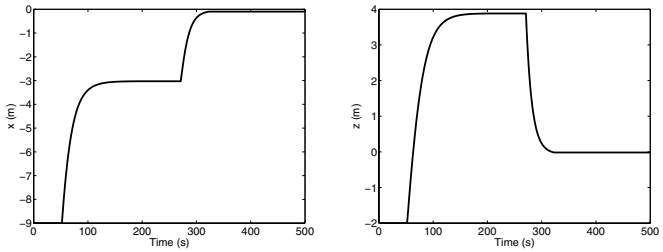

(a) Lateral motion (b) Forward motion

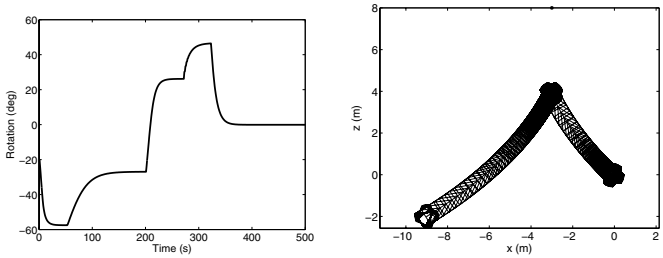

(c) Robot rotation (d) Path

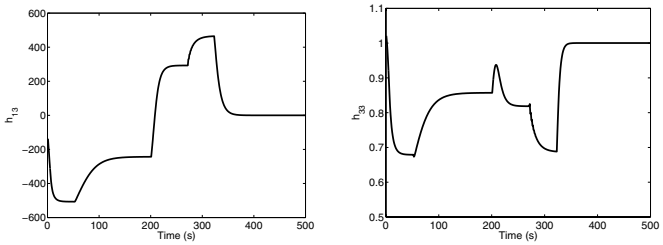

(e) h_{13} (f) h_{33}

Fig. 7. Simulation following two T-curves. (a-d) Robot coordinates and path. (e-f) Homography elements used in the control.

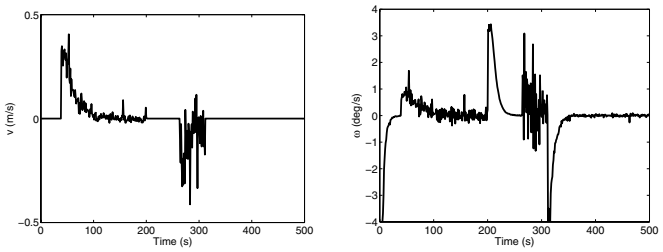

(a) Forward velocity (b) Angular velocity

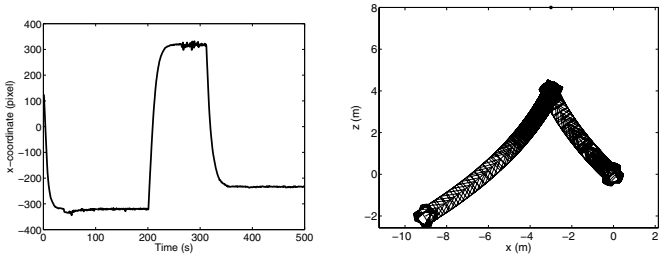

(c) x-coordinate of the target (d) Path

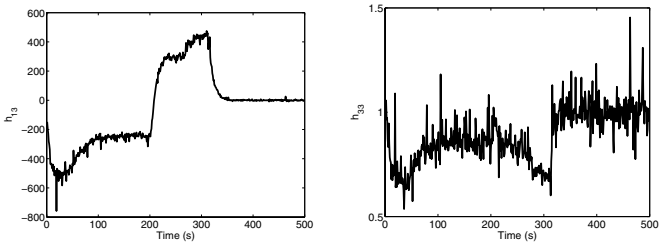

(e) h_{13} (f) h_{33}

Fig. 8. Simulation following two T-curves with image noise of $\sigma = 1$ pixel. (a-b) Output velocities. (c) x-coordinate of the observed target in the current image. (d) Robot path. (e-f) Homography elements used in the control.

next step. Given that the global switching control has been shown to be stable, the robot will finally converge to the goal. An example is shown in Fig. 9(b).

VI. CONCLUSIONS

A visual control scheme for differential drive vehicles is presented in this paper. This is a switched homography-based approach that takes into account the field-of-view camera constraints. Optimality in distance is the criteria for choosing the paths. Two types of paths with its respective controller are required, namely, one controller drives the robot along a straight line and the other drives the robot following T-curves until it reaches the goal. Stability analysis of both controllers is presented. The simulations carried out show that the approach works properly and simulations with image noise and odometry drift show good performance of the method. We also show that the control can easily cope with range constraints of the camera. In our opinion, combining motion-planning research with new visual control methods is a promising open field of future research.

APPENDIX

A. Control Selection: Decision of Regions

Before starting the navigation, we need to check what type of optimal path is required in order to select the proper control. In this section, we give the conditions on the ratio

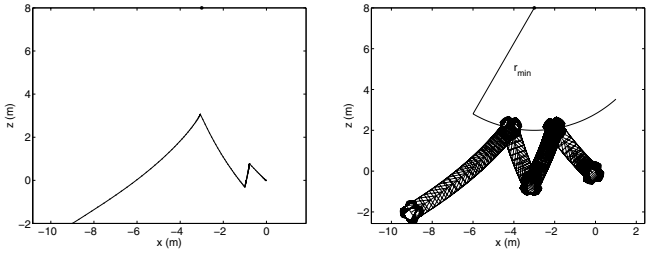

(a) (b)

Fig. 9. (a) Simulation of two iterations with odometry drift of 0.8 deg/m. Pose after each iteration: $(-1.00, -0.31, -2.63^\circ)$ and $(-0.02,\ -0.01,\ -0.05^\circ)$. (b) Simulation with minimum range constraint $r_{min} = 6$ m. Final pose $(-0.15, -0.08, -0.40^\circ)$.

$\frac{r_1}{r_2}$ (between initial and goal position) that decides the region where the goal lies with respect to the initial point. Let us derive the conditions for the goal to be on the boundary of the distinct regions. In the following discussion, P is the initial point and without loss of generality we can assume $P = (r_1, 0)$ in polar coordinates. Q is the goal point with polar coordinates (r_2, θ), where $0 \leq \theta \leq \pi$.

Consider Fig. 10 (left). Let us suppose Q lies on the boundary of region I. Applying *sine rule* in $\triangle PQO$ we obtain

$$\frac{r_2}{r_1} = \frac{\sin(\pi - |\,\phi_1\,|)}{\sin(|\,\phi_1\,| - \theta)} = \frac{\sin(|\,\phi_1\,|)}{\sin(|\,\phi_1\,| - \theta)}\,.$$

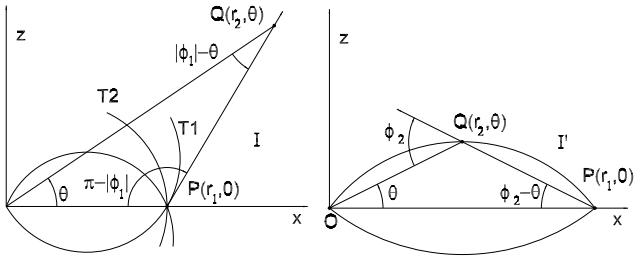

Fig. 10. Q on the boundary of region I (left) and region I' (right).

A necessary condition for Q to lie on the boundary of region I is $\theta <\mid \phi_1 \mid$. Hence the conditions for Q to lie on the boundary of region I are:

1) $\frac{r_2}{r_1} = \frac{\sin(|\phi_1|)}{\sin(|\phi_1|-\theta)}$
2) $\theta <\mid \phi_1 \mid$

Now consider Fig. 10 (right). Let us suppose Q lies on the boundary of region I'. Applying *sine rule* in $\triangle PQO$ we obtain

$$\frac{r_2}{r_1} = \frac{\sin(\phi_2 - \theta)}{\sin(\phi_2)} .$$

A necessary condition for Q to lie on the boundary of region I' is $\theta < \phi_2$. Hence the conditions for Q to lie on the boundary of region I' are:

1) $\frac{r_2}{r_1} = \frac{\sin(\phi_2-\theta)}{\sin(\phi_2)}$
2) $\theta < \phi_2$

If Q lies on a T1 or T2 curve, then, respectively,

$$\frac{r_2}{r_1} = e^{\frac{-\theta}{\tan\phi_1}} , \quad \frac{r_2}{r_1} = e^{\frac{-\theta}{\tan\phi_2}} . \tag{14}$$

A similar analysis can be done for the case $\theta \in [0, -\pi]$. Table I illustrates the criteria to decide the region in which Q lies based on the ratio $\frac{r_2}{r_1}$ and θ, where SL denotes a straight line path and $T1_p$, $T2_p$ denote the T-curves of point P.

TABLE I

TYPES OF OPTIMAL PATHS DEPENDING ON THE RATIO $\frac{r_2}{r_1}$ AND θ.

	$\frac{r_2}{r_1}$	$\mid \theta \mid$	Type of path
$\theta \in (-\pi, 0]$	$[0, \frac{\sin(\lvert\phi_1\rvert-\lvert\theta\rvert)}{\sin(\lvert\phi_1\rvert)}]$	$[0, \mid \phi_1 \mid]$	SL
	$[\frac{\sin(\lvert\phi_1\rvert-\lvert\theta\rvert)}{\sin(\lvert\phi_1\rvert)}, e^{\frac{\lvert\theta\rvert}{\tan\phi_1}}]$	$[0, \pi]$	$SL - T1_P$
	$[e^{\frac{\lvert\theta\rvert}{\tan\phi_1}}, e^{\frac{\lvert\theta\rvert}{\tan\phi_2}}]$	$[0, \pi]$	$T2_P * T1_P$
	$[e^{\frac{\lvert\theta\rvert}{\tan\phi_2}}, \frac{\sin(\phi_2)}{\sin(\phi_2-\lvert\theta\rvert)}]$	$[0, \phi_2]$	$SL - T2_P$
	$[\frac{\sin(\phi_2)}{\sin(\phi_2-\lvert\theta\rvert)}, \infty]$	$[0, \phi_2]$	SL
	$[e^{\frac{\lvert\theta\rvert}{\tan\phi_2}}, \infty]$	$[\phi_2, \pi]$	$SL - T1_P$
$\theta \in [0, \pi)$	$[0, \frac{\sin(\phi_2-\theta)}{\sin(\phi_2)}]$	$[0, \phi_2]$	SL
	$[\frac{\sin(\phi_2-\theta)}{\sin(\phi_2)}, e^{\frac{-\theta}{\tan\phi_2}}]$	$[0, \pi]$	$SL - T2_P$
	$[e^{\frac{-\theta}{\tan\phi_2}}, e^{\frac{-\theta}{\tan\phi_1}}]$	$[0, \pi]$	$T1_P * T2_P$
	$[e^{\frac{-\theta}{\tan\phi_1}}, \frac{\sin(\lvert\phi_1\rvert)}{\sin(\lvert\phi_1\rvert-\theta)}]$	$[0, \mid \phi_1 \mid]$	$SL - T1_P$
	$[\frac{\sin(\lvert\phi_1\rvert)}{\sin(\lvert\phi_1\rvert-\theta)}, \infty]$	$[0, \mid \phi_1 \mid]$	SL
	$[e^{\frac{-\theta}{\tan\phi_1}}, \infty]$	$[\mid \phi_1 \mid, \pi]$	$SL - T1_P$

REFERENCES

[1] R. Basri, E. Rivlin and I. Shimshoni, "Visual Homing: Surfing on the Epipoles ", *Int. J. of Computer Vision*, vol. 33, no. 2, 1999, 117-137.

[2] S. Benhimane and E. Malis, "Homography-based 2D Visual Servoing", *IEEE Int. Conf. on Robotics and Automation*, 2006, pp. 2397-2402.

[3] S. Benhimane, E. Malis, P. Rives and J. R. Azinheira, "Vision-based Control for Car Platooning using Homography Decomposition", *IEEE Int. Conference on Robotics and Automation*, 2005, pp. 2173-2178.

[4] S. Benhimane, E. Malis, "A new approach to vision-based robot control with omni-directional cameras", *IEEE International Conference on Robotics and Automation*, 2006, pp. 526-531.

[5] S. Bhattacharya, R. Murrieta-Cid and S. Hutchinson, "Optimal Paths for Landmark-based Navigation by Differential Drive Vehicles with Field-of-View Constraints", *IEEE Transactions on Robotics*, To appear, 2007.

[6] M. S. Branicky, "Multiple Lyapunov Functions and Other Analysis Tools for Switched and Hybrid Systems", *IEEE Transactions Automat. Control*, vol. 43, no. 4, 1998, pp. 475-482.

[7] E. Cervera, A. P. del Pobil, F. Berry, P. Martinet, "Improving Image-Based Visual Servoing with Three-Dimensional Features", *The International Journal of Robotics Research*, vol. 22, no. 10-11, October-November 2003, pp. 821-839.

[8] P. I. Corke and S. A. Hutchinson, "A New Partitioned Approach to Image-Based Visual Servo Control", *IEEE Trans. Robot. Autom.*, vol. 17, no. 4, 2001, pp. 507-515.

[9] G. N. DeSouza and A. C. Kak, "Vision for Mobile Robot Navigation: A Survey", *IEEE Trans. on Pattern Analysis and Machine Intelligence*, vol. 24, no. 2, 2002, pp. 237-267.

[10] Y. Fang, W. E. Dixon, D. M. Dawson and P. Chawda, "Homography-based visual servo regulation of mobile robots", *IEEE Trans. on Systems, Man, and Cybernetics*, vol. 35, no. 5, 2005, pp. 1041-1050.

[11] T. Ikeda and T. Mita and B. D. O. Anderson, "Position and attitude control of an underwater vehicle using variable constraint control", *IEEE Int. Conf. on Decision and Control*, 2001, pp. 3758-3763.

[12] T. Ikeda and T. Nam and T. Mita and B. D. O. Anderson, "Variable Constraint Control of Underactuated Free Flying Robots - Mechanical Design and Convergence", *IEEE International Conference on Decision and Control*, December, 1999, pp. 2539-2544.

[13] R. I. Hartley and A. Zisserman, *Multiple View Geometry in Computer Vision*, Cambridge University Press, 2004.

[14] S. Hutchinson, G. Hager, and P. I. Corke, "A Tutorial on Visual Servo Control", *IEEE Trans. on Robotics and Automation*, vol. 12, no. 5, Oct. 1996, pp. 651-670.

[15] G. Kantor and Alfred A. Rizzi, "Feedback Control of Underactuated Systems via Sequential Composition: Visually Guided Control of a Unicycle", *Proc. of 11th Int. Symposium of Robotics Research*, 2003.

[16] J. P. Laumond, *Robot Motion Planning and Control*, Lectures Notes in Control and Information Sciences 229. Springer, 1998.

[17] G. López-Nicolás, C. Sagüés, J.J. Guerrero, D. Kragic and P. Jensfelt, "Nonholonomic Epipolar Visual Servoing", *IEEE Int. Conf. on Robotics and Automation*, 2006, pp. 2378-2384.

[18] G. López-Nicolás, C. Sagüés and J.J. Guerrero, "Homography-Based Visual Servoing for Nonholonomic Robots", *Technical report, DIIS-I3A, Universidad de Zaragoza*, no. V06.1, July 2006.

[19] E. Malis, F. Chaumette and S. Boudet, "2 1/2 D Visual Servoing", *IEEE Trans. on Robotics and Aut.*, vol. 15, no. 2, 1999, pp. 234-246.

[20] Y. Mezouar and F. Chaumette, "Path Planning for Robust Image-Based Control", *IEEE Trans. on Robotics and Automation*, vol. 18, no. 4, August 2002, pp. 534-549.

[21] Y. Mezouar and F. Chaumette, "Optimal Camera Trajectory with Image-Based Control", *The International Journal of Robotics Research*, vol. 22, no. 10-11, October-November 2003, pp. 781-803.

[22] P. Rives, "Visual Servoing Based on Epipolar Geometry", *IEEE/RSJ Int. Conf. on Intelligent Robots and Systems*, vol. 1, 2000, pp. 602-607.

[23] C. Sagüés and J.J. Guerrero, "Visual correction for mobile robot homing", *Robotics and Autonomous Systems*, vol. 50, no. 1, 2005, pp. 41-49.

[24] J. Weng, T.S. Huang and N. Ahuja, *Motion and Structure from Image Sequences*, Springer-Verlag, 1993.

[25] H. Zhang and J. P. Ostrowski, "Visual Motion Planning for Mobile Robots", *IEEE Transactions on Robotics and Automation*, vol. 18, no. 2, April 2002, pp. 199-208.